This is the accepted manuscript made available via CHORUS. The article has been published as:

Phenomenology of Spectral Functions in Disordered Spin Chains at Infinite Temperature

Lev Vidmar, Bartosz Krajewski, Janez Bonča, and Marcin Mierzejewski

Phys. Rev. Lett. **127**, 230603 — Published 1 December 2021

DOI: 10.1103/PhysRevLett.127.230603

Phenomenology of spectral functions in disordered spin chains at infinite temperature

Lev Vidmar,[1,2] Bartosz Krajewski,[3] Janez Bonča,[2,1] and Marcin Mierzejewski[3]

[1] *Department of Theoretical Physics, J. Stefan Institute, SI-1000 Ljubljana, Slovenia*
[2] *Department of Physics, Faculty of Mathematics and Physics, University of Ljubljana, SI-1000 Ljubljana, Slovenia*
[3] *Department of Theoretical Physics, Faculty of Fundamental Problems of Technology, Wrocław University of Science and Technology, 50-370 Wrocław, Poland*

Studies of disordered spin chains have recently experienced a renewed interest, inspired by the question to which extent the exact numerical calculations comply with the existence of a many-body localization phase transition. For the paradigmatic random field Heisenberg spin chains, many intriguing features were observed when the disorder is considerable compared to the spin interaction strength. Here, we introduce a phenomenological theory that may explain some of those features. The theory is based on the proximity to the noninteracting limit, in which the system is an Anderson insulator. Taking the spin imbalance as an exemplary observable, we demonstrate that the proximity to the local integrals of motion of the Anderson insulator determines the dynamics of the observable at infinite temperature. In finite interacting systems our theory quantitatively describes its integrated spectral function for a wide range of disorders.

Introduction. A considerable effort has been devoted to understanding the emergence of ergodicity in physically relevant quantum many-body systems. Important cornerstones are provided by the random matrix theory (RMT) and the eigenstate thermalization hypothesis (ETH) [1–6]. Even though a rigorous proof of the ETH is still missing, several exact numerical studies confirmed its validity with remarkable accuracy, at least for specific parameter regimes of some physical Hamiltonians [4, 7–18]. The clearest numerical results have been obtained for the regimes where all model parameters are quantitatively similar and the numerical artifacts are strongly suppressed. Much less understood are properties of many-body systems in which some physical processes (e.g., interaction or quenched disorder) are dominant over all other processes. Exciting open questions concern the possibility of ergodicity breaking phase transitions and a generalization of the KAM theorem [19–21]. In strongly disordered systems, this type of ergodicity breaking phase transition is referred to as the many-body localization transition [22–28].

A recent study [29] argued that the identification of ergodicity in numerical results may strongly depend on the value of the Thouless time $t_{\rm Th}$ relative to the Heisenberg time $t_{\rm H}$ [30]. A system is interpreted as ergodic if $t_{\rm Th} \ll t_{\rm H}$, while in the opposite regime $t_{\rm Th} \gtrsim t_{\rm H}$ the interpretation of finite-size results appears to be less conclusive. For a quantitative illustration, let us consider the random field Heisenberg chain with L sites,

$$\hat{H} = J \sum_i (\hat{S}_i^x \hat{S}_{i+1}^x + \hat{S}_i^y \hat{S}_{i+1}^y + \Delta \hat{S}_i^z \hat{S}_{i+1}^z) + \sum_i h_i \hat{S}_i^z, \quad (1)$$

where $\hat{S}_i^\alpha$ ($\alpha = x, y, z$) are standard spin-1/2 operators and the local fields h_i (in units of $J \equiv 1$) are independent and identically distributed random variables drawn from the box distribution, $h_i \in [-W, W]$. It was shown [29] that in finite systems ($L \lesssim 20$) at $\Delta = 1$, the criterion $t_{\rm Th} \sim t_{\rm H}$ is satisfied around $W = W^* \approx 2$. Considering the behavior of the system (1) with increasing disorder strength W, this point can therefore be interpreted as the onset of the ergodicity breakdown. The latter is consistent with the level statistics and the eigenstate entanglement entropies departing from the RMT predictions [31], the fidelity susceptibility being maximal [32], the distribution of observable matrix elements being anomalous [33, 34], the opening of the Schmidt gap [35] and the gap in the spectrum of the eigenstate one-body density matrix [36], and the correlation-hole time in the survival probability reaching $t_{\rm H}$ [37].

Despite those developments, the fate of the ergodicity breaking point in the thermodynamic limit remains an extensively debated topic [29, 31–33, 38–40]. Moreover, previous studies reported other fascinating phenomena such as subdiffusive transport [41–47] and an approximate $1/\omega$ scaling of the spin density spectral function [32, 48, 49]. These observations call for a universal description within a simple theory that should provide quantitative predictions at all disorder strengths.

In this Letter we introduce a phenomenological theory that may achieve some of those goals. We develop the theory on the premise that the noninteracting point at $\Delta = 0$, which is Anderson localized for any disorder in the thermodynamic limit [50, 51], determines specific properties of disordered spin chains also at $\Delta \neq 0$. The key ingredient of the theory is the proximity to the local integrals of motion of the Anderson insulator (shortly, Anderson LIOMs). In particular, we allow the Anderson LIOMs to acquire a finite relaxation time due to interactions, i.e., they may become delocalized. The theory provides an analytical description of the frequency dependence of the spectral function, it exhibits a remarkable agreement with numerical results for a wide range of disorders, and it suggests that at least a fraction of Anderson LIOMs are delocalized. Specifically, for the spin imbalance observable, we explain rich phenomenology of the spectral function, which ranges from the anomalous $\approx 1/\omega$ behavior at moderate disorders to more complicated functional forms at strong disorder.

Spectral function. The central quantity in our studies is the spectral function $S(\omega)$ of an observable $\hat{A}$, which is the Fourier transform of its autocorrelation function,

$$S(\omega) = \frac{1}{2\pi}\int_{-\infty}^{\infty} \mathrm{d}t\; e^{i\omega t - |t|0^+} \langle e^{i\hat{H}t}\hat{A}e^{-i\hat{H}t}\hat{A}\rangle\,, \quad (2)$$

where $\langle\cdots\rangle = \mathrm{Tr}\{\cdots\}/\mathcal{D}$ denotes the ensemble average over all eigenstates and $\mathcal{D}$ is the dimension of the Hilbert space. Our numerical calculations are carried out for its integral

$$I(\omega) = \int_{-\omega}^{\omega} \mathrm{d}\omega' S(\omega') = \frac{1}{\mathcal{D}}\sum_{m,n=1}^{\mathcal{D}} \theta\left(\omega - |E_m - E_n|\right) A_{mn}^2\,, \quad (3)$$

where E_n are the energy levels and $A_{mn} \equiv \langle m|\hat{A}|n\rangle$ are matrix elements of $\hat{A}$ in the eigenstate basis, $\hat{H}|n\rangle = E_n|n\rangle$, θ is the Heaviside step function, and we set $\hbar \equiv 1$. We study observables that are traceless, $\langle\hat{A}\rangle = 0$, and normalized, $||\hat{A}||^2 = \langle\hat{A}\hat{A}\rangle = 1$ [14]. As a consequence, the high-frequency limit of $I(\omega)$ equals $\lim_{\omega\to\infty} I(\omega) = \frac{1}{\mathcal{D}}\sum_{m,n} A_{mn}^2 = \langle\hat{A}\hat{A}\rangle = 1$.

The integrated spectral function $I(\omega)$ filters out fast fluctuations and thereby allows for a robust analysis of the dynamics encoded in $I(\omega)$ even for a single realization of disorder. A particular observable that we study is the spin imbalance, $\hat{A} = \frac{2}{\sqrt{L}}\sum_i (-1)^i \hat{S}_i^z$. This observable has been measured experimentally [52, 53], it is a self-averaging quantity in macroscopic systems, and it has nonvanishing projections on multiple Anderson LIOMs. In the language of [54], this observable is integrability preserving in the noninteracting limit $\Delta = 0$.

Comparison with the noninteracting limit. Figure 1(a) shows $I(\omega)$ for a single realization of disorder at $\Delta = 1$ (examples for other realizations are shown in [55]). Results are compared to the noninteracting system, $I_0(\omega)$ at $\Delta = 0$. For $\omega > J$ the results are qualitatively very similar, while important differences emerge in the low-frequency regime $\omega \ll J$, which is the main interest of this work.

The spectral weight of the Anderson insulator in the low-ω regime is strongly suppressed, which is manifested as $I_0(\omega \ll J) \simeq$ const. This can be interpreted as the accumulation of the spectral weight of the observable in the stiffness $D_0 = \lim_{\omega\to 0^+} I_0(\omega)$, and hence the spectral function can be approximated as $S_0(\omega \ll J) \simeq D_0\delta(\omega)$. In contrast, the low-$\omega$ spectral weight of the interacting system may be considerable since $I(\omega \ll J) \neq$ const. This property gives rise to the *anomalous dynamics* of the imbalance for $\Delta \neq 0$ and $\omega \ll J$ [32, 45, 48, 49, 56–61], and is the main focus of this Letter.

As an important detail relevant for subsequent analysis, we note that the stiffness D_0 of an *arbitrary* observable $\hat{A}$ in the Anderson insulator ($\Delta = 0$) originates from its projections on the Anderson LIOMs $\{\hat{Q}_\alpha\}$. Therefore,

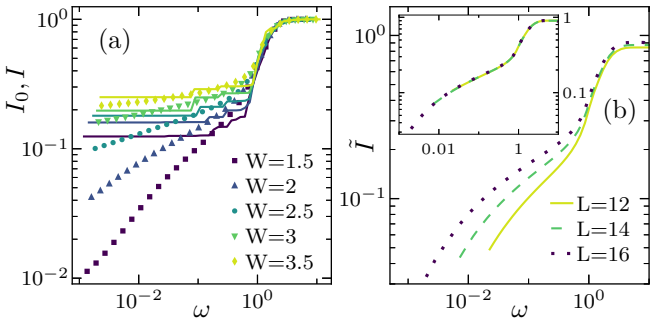

FIG. 1. (a) Integrated spectral functions $I(\omega)$ [$\Delta = 1$, symbols] and $I_0(\omega)$ [$\Delta = 0$, lines] at $L = 16$. Results are shown for a single disorder realization and various values of W, such that the ratio h_i/W in Eq. (1) is independent of W. (b) Regular part $\tilde{I}(\omega)$, averaged over 10^3 realizations of the disorder at $W = 2$. The results for $L = 12$ and 14 in the inset are shifted upwards by a constant to overlap with the data for $L = 16$. We set $J \equiv 1$ in all figures, and consider periodic boundary conditions in (1).

the spectral function for $\omega \ll J$ can be written as

$$S_{\mathrm{M},0}(\omega) = \sum_\alpha D_\alpha \delta(\omega)\,, \quad D_\alpha = \frac{\langle\hat{A}\hat{Q}_\alpha\rangle^2}{\langle\hat{Q}_\alpha\hat{Q}_\alpha\rangle}\,, \quad (4)$$

where $D_0 = \sum_\alpha D_\alpha$. The latter relation follows from the Mazur bound [14], and we consider the Anderson insulator as an integrable model containing orthogonal Anderson LIOMs $\langle\hat{Q}_\alpha\hat{Q}_{\alpha'}\rangle \propto \delta_{\alpha,\alpha'}$ (see [55] for details about the Anderson LIOMs). Since the projections D_α are defined in Eq. (4) by the average over the entire Hilbert space, we do not study the energy-resolved spectral functions, but instead we focus on the infinite temperature at which the average energy $(E_m + E_n)/2$ in Eq. (3) is arbitrary.

Low-frequency regime. In what follows we focus on the interacting systems ($\Delta = 1$), and we disentangle the effect of accumulation of spectral weight in the stiffness from the low-ω spectral weight. To this end, we study the *regular* part of the integrated spectral function, defined as $\tilde{I}(\omega) = I(\omega) - \frac{1}{\mathcal{D}}\sum_{n=1}^{\mathcal{D}} A_{nn}^2$. An example of the disorder averaged $\tilde{I}(\omega)$ at $W = 2$ and different system sizes L is shown in Fig. 1(b). It is remarkable that a simple upward shift of the curves for $L = 12$ and 14 results in an accurate overlap with the data for $L = 16$. This is observed at $W = 2$ in the inset of Fig. 1(b), and other values of the disorder in [55]. This suggests that the finite-size effects in the low-ω regime are small (apart from the L-dependent vertical shift), and calls for a simple theory to describe the observable spectral function.

An interesting remark can be made about the overlap of integrated spectral functions such as the one in the inset of Fig. 1(b). It indicates that a fraction of the spectral weight from the diagonal matrix elements at $\delta(\omega)$ is transferred to nonzero frequencies with increasing L. This may be interpreted as the trend towards restoring

the ergodicity in the thermodynamic limit. Several works have recently explored possibilities for restoring the ergodicity at large disorders when the thermodynamic limit is approached [29, 31, 32, 62–64]. Nevertheless, our main focus here is to provide quantitative predictions for properties in *finite* systems.

Proximity to Anderson insulator. We now construct a phenomenological theory that may quantitatively describe the observable spectral functions in finite systems. Our approach is based on the proximity to the Anderson insulator whose conserved quantities are denoted as Anderson LIOMs. Anderson LIOMs considered here do not imply existence of l-bits in interacting systems [65–72]. The key premise of the theory is the conjecture that upon interactions, at least a fraction of Anderson LIOMs $\{\hat{Q}_\alpha\}$ become delocalized, i.e., they cease to be conserved and $\langle \hat{Q}_\alpha(t)\hat{Q}_\alpha\rangle$ decays with a finite relaxation time τ_α. This impacts the dynamics of finite systems by broadening the δ-functions in Eq. (4). We model this effect by the following regular part of the spectral function for interacting system [cf. Eq. (4)],

$$S_{\rm M}(\omega \ll J) = \sum_{\alpha=1}^{N} D_\alpha \frac{1}{\pi}\frac{\tau_\alpha}{(\omega\tau_\alpha)^2+1}\,, \tag{5}$$

where the summation runs over N Anderson LIOMs that have nonvanishing projections on $\hat{A}$ and are delocalized in the interacting system. Note that the broadening in Eq. (5) is described by the Lorentzian functions, which is a common approach in the literature. Recently, the Lorentzian form of the spectral function [cf. Eq. (5) with $N = 1$] was actually observed in numerical studies of several many-body systems close to integrable points [17, 64, 73]. Nevertheless, we argue in [55] that the main results of our study are independent of the particular functional form of the broadening function.

An important input to the theory are the values of the stiffnesses $\{D_\alpha\}$ and the relaxation times $\{\tau_\alpha\}$ of delocalized Anderson LIOMs in the Hamiltonian (1). We calculated both quantities numerically at disorders $W = 2$ and 3, see Sec. S4 of [55]. The first insight is that, for the spin imbalance, many projections D_α from Eq. (4) are nonzero, and hence one needs to consider $N \gg 1$ in Eq. (5). The second insight is that the projections are very weakly correlated (or uncorrelated) with the relaxation times, and hence we replace D_α with its average value in Eq. (5), $D_\alpha \to 1/N\sum_\alpha D_\alpha = D_0/N$. Finally, we calculated the distribution $f_\tau(\tau)$ of the relaxation times τ_α of the autocorrelation functions $\langle \hat{Q}_\alpha(t)\hat{Q}_\alpha\rangle$ and found that the distribution $f_\tau(\tau)$ is extremely wide. In particular, the distribution can be well approximated by a power-law dependence $f_\tau(\tau) \propto 1/\tau^\mu$ in an interval $\tau \in [\tau_{\rm min}, \tau_{\rm max}]$, where the disorder strength only impacts the exponent μ and the boundaries $\tau_{\rm min}$ and $\tau_{\rm max}$. Such a power-law distribution of relaxation times τ_α is consistent with the distributions of τ_α studied for the Anderson insulators coupled to regular bosons or hard-core bosons via the Fermi golden rule [74, 75].

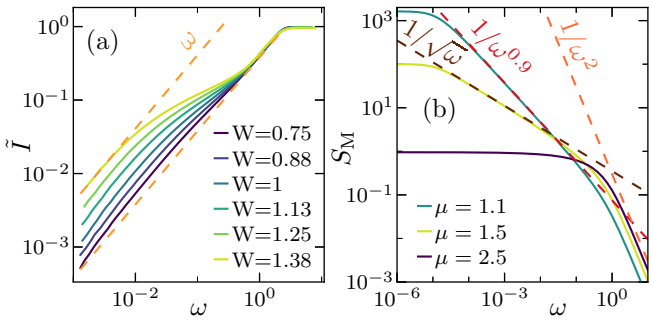

FIG. 2. (a) Numerical results for the regular part of the integrated spectral function $\tilde{I}(\omega)$ at $L = 16$ and weak disorder. Results are averaged over 10^3 realizations of disorder. (b) Solid lines: $S_{\rm M}(\omega)$ from Eq. (6) at $\mu = 1.1$, 1.5 and 2.5, using $\tau_{\rm min} = 1$, $\tau_{\rm max} = 10^5$ and $\bar{D}_0 = 1$. Dashed lines are approximate power-law fits.

Summarizing the above considerations, we replace the sum $N^{-1}\sum_{\alpha=1}^{N}$ in Eq. (5) with the integral $\int_{\tau_{\rm min}}^{\tau_{\rm max}} {\rm d}\tau f_\tau(\tau)$, and obtain a phenomenological model to describe the low-frequency dynamics,

$$S_{\rm M}(\omega) = \frac{\bar{D}_0}{\pi}\int_{\tau_{\rm min}}^{\tau_{\rm max}} \frac{{\rm d}\tau}{\tau^{\mu-1}}\frac{1}{(\omega\tau)^2+1}\,, \tag{6}$$

where $\bar{D}_0$ is a prefactor that determines the total spectral weight arising from the delocalized Anderson LIOMs. In analogy to Eq. (3), we then define $\tilde{I}_{\rm M}(\omega)$ by the integral of $S_{\rm M}(\omega)$, see also [55].

Before carrying out a quantitative comparison of our phenomenological model with the actual numerical data, we comment on some general properties of the spectral function described by Eq. (6). We first note that if $\omega \ll \tau_{\rm max}^{-1}$, then $S_{\rm M}(\omega) \propto$ const and $\tilde{I}(\omega) \propto \omega$. This property is usually associated with the diffusive character of the dynamics. Emergence of such regime was detected in several studies of many-body systems that comply with the ETH [4, 15–17, 64, 76–78]. For the model under investigation, see Fig. 2(a), we indeed observe $\tilde{I}(\omega) \propto \omega$ at $W \approx 1$. In this regime of parameters, the phenomenological model (6) can be simplified since $\tau_{\rm min}$ and $\tau_{\rm max}$ are of the same order and hence one may use a single relaxation time, $\tau_\alpha \to \tau$. With increasing the disorder W, however, the linear regime in $\tilde{I}(\omega)$ shifts to lower ω, which is a consequence of a rapid increase of $\tau_{\rm max}$ with W.

The main message of this Letter is that, for a wide range of disorder strengths, the low-frequency response may be governed by a broad distribution of the relaxation times $\{\tau_\alpha\}$, with $\tau_{\rm max}/\tau_{\rm min} \gg 1$ in Eq. (6). This suggests that the frequency regime $\tau_{\rm max}^{-1} \ll \omega \ll \tau_{\rm min}^{-1}$ may be very broad and hence relevant for the time regimes studied in numerical simulations and analog quantum simulators [52, 53]. Particularly informative is the case $\mu = 1$

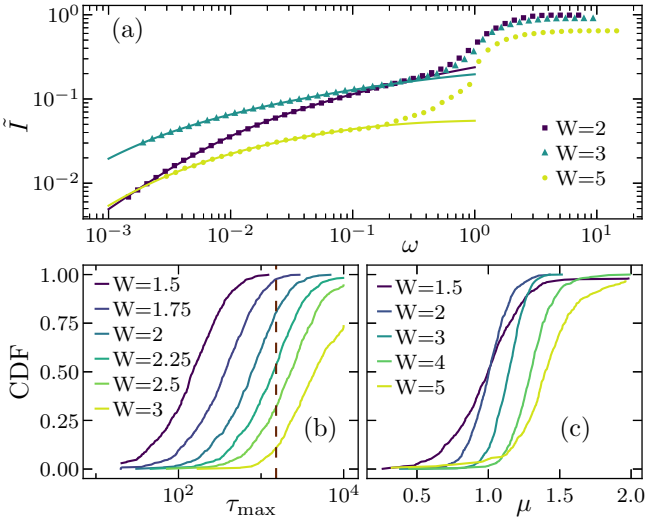

FIG. 3. (a) Symbols: numerical results for $\tilde{I}(\omega)$ at $L = 16$ and a single realization of the disorder W. Lines: predictions by $\tilde{I}_M(\omega)$ for the low-frequency regime $\omega < 0.2$. (b) and (c) The resulting cumulative distribution functions (CDF) of the fitting parameters $\tau_{\max}$ and μ, respectively, for 10^3 realizations of the disorder. The vertical dashed line in (b) denotes the Heisenberg time $t_{\rm H}$ at $W = 2$. See [55] for details.

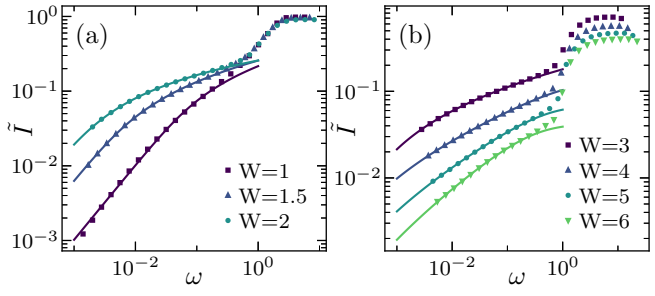

FIG. 4. Symbols: numerical results for the disorder averages of $\tilde{I}(\omega)$ at $L = 16$, using 10^3 disorder realizations. Lines: predictions by $\tilde{I}_M(\omega)$ for the low-frequency regime $\omega < 0.2$. See [55] for details.

in Eq. (6), for which

$$S_{\rm M}(\omega) = \frac{\bar{D}_0}{\pi} \frac{\arctan(\omega\tau_{\max}) - \arctan(\omega\tau_{\min})}{\omega} . \quad (7)$$

The functional form $\propto 1/\omega$ at $\mu = 1$ is consistent with the anomalous dynamics and spectral functions reported in several previous studies [32, 48, 49]. More generally, $S_{\rm M}(\omega)$ at $\mu < 2$ can roughly be approximated by $S_{\rm M}(\omega) \propto 1/\omega^{\eta}$ with $\eta \simeq 2 - \mu$, see Fig. 2(b) for $\mu = 1.1$ and 1.5. In [55] we show that the $1/\omega^{\eta}$ dependence arises solely from the power-law distribution of relaxation times $\{\tau_\alpha\}$, and is not an artifact of the Lorentzian broadening used in Eq. (5). We note, however, that the functional forms predicted by Eq. (6), as well as the numerical results in Figs. 3 and 4, may also exhibit a fine structure beyond a simple power-law dependence. In the opposite regime $\mu > 2$, $S_{\rm M}(\omega)$ resembles a Fourier transform of a single Lorentzian, as shown in Fig. 2(b) for $\mu = 2.5$.

Numerical tests for spin imbalance. We now carry out a quantitative comparison between the numerical results for $\tilde{I}(\omega)$ [symbols in Figs. 3 and 4] and the predictions $\tilde{I}_{\rm M}(\omega)$ from the phenomenological model in Eq. (6) [lines in Figs. 3(a) and 4]. The fitting parameters of the latter are $\tau_{\min}$, $\tau_{\max}$ and μ that determine the distribution of relaxation times, and the prefactor $\bar{D}_0$.

Figure 3 considers the case where the free parameters of $\tilde{I}_{\rm M}(\omega)$ are fitted independently for every disorder realization. An example of the outcome of such procedure is shown in Fig. 3(a) for a single disorder realization, while examples for several other realizations are shown in [55]. Figures 3(b) and 3(c) then show the cumulative distribution of fitting parameters obtained by analyzing 10^3 realizations of disorder. There are two important quantitative results. The first is that the distribution of $\tau_{\max}$ is broad and its mean increases approximately exponentially with W, unless it reaches the Heisenberg time $t_{\rm H} = \omega_{\rm H}^{-1}$ at $W^* \approx 2$, see the vertical line in Fig. 3(b). (The Heisenberg energy $\omega_{\rm H}$ corresponds to the average level spacing in the middle of the spectrum, which at $L = 16$ is $\omega_{\rm H}/J \approx 10^{-3}$ [29].) The value $W^* \approx 2$ is consistent with the ergodicity breaking transition point in this model, occurring when the Thouless time $t_{\rm Th}$ in the spectral form factor approaches $t_{\rm H}$ [31]. When $\tau_{\max}$ exceeds $t_{\rm H}$, the mean of μ departs from $\mu = 1$ towards higher values [see Fig. 3(c)]. The second important result is that $\tau_{\min}$ remains well below $t_{\rm H}$ for all results reported here. Otherwise, the dynamics would be frozen, $\tilde{I}(\omega) \simeq$ const, down to $\omega \sim \omega_{\rm H}$, which is clearly not the case in Figs. 3(a) or 4(b). The first result suggests that a fraction of Anderson LIOMs remains localized at $W > W^*$ upon adding the interactions. Exploring the fate of those LIOMs for larger systems, i.e., when $t_{\rm H} \to \infty$, is beyond the scope of this work. The second result suggests that at least some fraction of Anderson LIOMs is delocalized in the interacting system for all disorder values considered here. In Fig. 4 we carry out an analogous analysis for the disorder averages of $\tilde{I}(\omega)$. Also in this case, the phenomenological model from Eq. (6) provides an extremely accurate description of the results. A quantitative analysis of the fitting parameters $\tau_{\max}$ and μ is provided in [55].

Conclusions. In this Letter we introduced a phenomenological theory that accurately describes the spectral properties of the spin imbalance in disordered chains. The theory is based on the proximity to the Anderson insulator, in which the long-time dynamics is strongly suppressed as compared to the interacting system. We assume that the anomalous long-time dynamics of the interacting systems arises from certain Anderson LIOMs that acquire a finite relaxation times. An important ingredient of the underlying phenomenological model is a broad distribution of relaxation times of Anderson LIOMs. Then in finite systems amenable to exact diagonalization there exist the disorder W^* [$W^* \approx 2$ for the

model in (1)], above which the relaxation times $\{\tau_\alpha\}$ of a fraction of Anderson LIOMs are larger than the Heisenberg time $t_{\rm H}$. As a result the properties of finite systems at $W > W^*$ are governed by the coexistence of two types of LIOMs: those for which $\tau_\alpha > t_{\rm H}$ (they appear to be exactly conserved), and those for which $\tau_\alpha < t_{\rm H}$ (they cease to be conserved due to interactions). The interplay between both types of LIOMs may give rise to unconventional properties of the system defined on a Fock space graph [79–84], which needs to be explored in more details in future work.

ACKNOWLEDGMENTS

We acknowledge discussions with F. Heidrich-Meisner, D. Logan, A. Polkovnikov, T. Prosen, M. Rigol, D. Sels and P. Sierant. We acknowledge the support by the National Science Centre, Poland via project 2020/37/B/ST3/00020 (M.M.), the support by the Slovenian Research Agency (ARRS), Research Core Fundings Grants P1-0044 (L.V. and J.B.) and J1-1696 (L.V.), and the support from the Center for Integrated Nanotechnologies, a U.S. Department of Energy, Office of Basic Energy Sciences user facility (J.B.).

[1] J. M. Deutsch, Quantum statistical mechanics in a closed system, Phys. Rev. A **43**, 2046 (1991).
[2] M. Srednicki, Chaos and quantum thermalization, Phys. Rev. E **50**, 888 (1994).
[3] M. Rigol, V. Dunjko, and M. Olshanii, Thermalization and its mechanism for generic isolated quantum systems, Nature (London) **452**, 854 (2008).
[4] L. D'Alessio, Y. Kafri, A. Polkovnikov, and M. Rigol, From quantum chaos and eigenstate thermalization to statistical mechanics and thermodynamics, Adv. Phys. **65**, 239 (2016).
[5] T. Mori, T. N. Ikeda, E. Kaminishi, and M. Ueda, Thermalization and prethermalization in isolated quantum systems: a theoretical overview, J. Phys. B **51**, 112001 (2018).
[6] J. M. Deutsch, Eigenstate thermalization hypothesis, Rep. Prog. Phys. **81**, 082001 (2018).
[7] L. F. Santos and M. Rigol, Onset of quantum chaos in one-dimensional bosonic and fermionic systems and its relation to thermalization, Phys. Rev. E **81**, 036206 (2010).
[8] W. Beugeling, R. Moessner, and M. Haque, Finite-size scaling of eigenstate thermalization, Phys. Rev. E **89**, 042112 (2014).
[9] R. Steinigeweg, A. Khodja, H. Niemeyer, C. Gogolin, and J. Gemmer, Pushing the limits of the eigenstate thermalization hypothesis towards mesoscopic quantum systems, Phys. Rev. Lett. **112**, 130403 (2014).
[10] H. Kim, T. N. Ikeda, and D. A. Huse, Testing whether all eigenstates obey the eigenstate thermalization hypothesis, Phys. Rev. E **90**, 052105 (2014).
[11] R. Mondaini and M. Rigol, Eigenstate thermalization in the two-dimensional transverse field Ising model. II. Off-diagonal matrix elements of observables, Phys. Rev. E **96**, 012157 (2017).
[12] D. Jansen, J. Stolpp, L. Vidmar, and F. Heidrich-Meisner, Eigenstate thermalization and quantum chaos in the Holstein polaron model, Phys. Rev. B **99**, 155130 (2019).
[13] T. LeBlond, K. Mallayya, L. Vidmar, and M. Rigol, Entanglement and matrix elements of observables in interacting integrable systems, Phys. Rev. E **100**, 062134 (2019).
[14] M. Mierzejewski and L. Vidmar, Quantitative impact of integrals of motion on the eigenstate thermalization hypothesis, Phys. Rev. Lett. **124**, 040603 (2020).
[15] M. Brenes, T. LeBlond, J. Goold, and M. Rigol, Eigenstate Thermalization in a Locally Perturbed Integrable System, Phys. Rev. Lett. **125**, 070605 (2020).
[16] J. Richter, A. Dymarsky, R. Steinigeweg, and J. Gemmer, Eigenstate thermalization hypothesis beyond standard indicators: Emergence of random-matrix behavior at small frequencies, Phys. Rev. E **102**, 042127 (2020).
[17] C. Schönle, D. Jansen, F. Heidrich-Meisner, and L. Vidmar, Eigenstate thermalization hypothesis through the lens of autocorrelation functions, arXiv:2011.13958.
[18] M. Brenes, S. Pappalardi, M. T. Mitchison, J. Goold, and A. Silva, Out-of-time-order correlations and the fine structure of eigenstate thermalisation, arXiv:2103.01161.
[19] A. N. Kolmogorov, On Conservation of Conditionally Periodic Motions for a Small Change in Hamilton's Function, Dokl. Akad. Nauk SSSR **98**, 527 (1954).
[20] J.-S. Caux and J. Mossel, Remarks on the notion of quantum integrability, J. Stat. Mech. **2011**, P02023 (2011).
[21] G. P. Brandino, J.-S. Caux, and R. M. Konik, Glimmers of a quantum KAM theorem: Insights from quantum quenches in one-dimensional bose gases, Phys. Rev. X **5**, 041043 (2015).
[22] D. Basko, I. Aleiner, and B. Altshuler, Metal-insulator transition in a weakly interacting many-electron system with localized single-particle states, Ann. Phys. **321**, 1126 (2006).
[23] I. V. Gornyi, A. D. Mirlin, and D. G. Polyakov, Interacting electrons in disordered wires: Anderson localization and low-T transport, Phys. Rev. Lett. **95**, 206603 (2005).
[24] A. Pal and D. A. Huse, Many-body localization phase transition, Phys. Rev. B **82**, 174411 (2010).
[25] R. Nandkishore and D. A. Huse, Many-body-localization and thermalization in quantum statistical mechanics, Ann. Rev. Cond. Mat. Phys. **6**, 15 (2015).

[26] E. Altman and R. Vosk, Universal dynamics and renormalization in many-body-localized systems, Ann. Rev. Cond. Mat. Phys. **6**, 383 (2015).

[27] F. Alet and N. Laflorencie, Many-body localization: An introduction and selected topics, C. R. Physique **19**, 498 (2018).

[28] D. A. Abanin, E. Altman, I. Bloch, and M. Serbyn, Colloquium: Many-body localization, thermalization, and entanglement, Rev. Mod. Phys. **91**, 021001 (2019).

[29] J. Šuntajs, J. Bonča, T. Prosen, and L. Vidmar, Quantum chaos challenges many-body localization, Phys. Rev. E **102**, 062144 (2020).

[30] The Thouless time t_{Th} may be seen as the longest physically relevant relaxation time, and the Heisenberg time t_{H} is proportional to the inverse level spacing.

[31] J. Šuntajs, J. Bonča, T. Prosen, and L. Vidmar, Ergodicity breaking transition in finite disordered spin chains, Phys. Rev. B **102**, 064207 (2020).

[32] D. Sels and A. Polkovnikov, Dynamical obstruction to localization in a disordered spin chain, arXiv:2009.04501.

[33] R. K. Panda, A. Scardicchio, M. Schulz, S. R. Taylor, and M. Žnidarič, Can we study the many-body localisation transition?, EPL **128**, 67003 (2020).

[34] Á. L. Corps, R. A. Molina, , and A. Relaño, Signatures of a critical point in the many-body localization transition, SciPost Phys. **10**, 107 (2021).

[35] J. Gray, S. Bose, and A. Bayat, Many-body localization transition: Schmidt gap, entanglement length, and scaling, Phys. Rev. B **97**, 201105 (2018).

[36] S. Bera, H. Schomerus, F. Heidrich-Meisner, and J. H. Bardarson, Many-body localization characterized from a one-particle perspective, Phys. Rev. Lett. **115**, 046603 (2015).

[37] M. Schiulaz, E. J. Torres-Herrera, and L. F. Santos, Thouless and relaxation time scales in many-body quantum systems, Phys. Rev. B **99**, 174313 (2019).

[38] P. Sierant, D. Delande, and J. Zakrzewski, Thouless Time Analysis of Anderson and Many-Body Localization Transitions, Phys. Rev. Lett. **124**, 186601 (2020).

[39] P. Sierant, M. Lewenstein, and J. Zakrzewski, Polynomially filtered exact diagonalization approach to many-body localization, Phys. Rev. Lett. **125**, 156601 (2020).

[40] D. Abanin, J. Bardarson, G. De Tomasi, S. Gopalakrishnan, V. Khemani, S. Parameswaran, F. Pollmann, A. Potter, M. Serbyn, and R. Vasseur, Distinguishing localization from chaos: Challenges in finite-size systems, Annals of Physics **427**, 168415 (2021).

[41] Y. Bar Lev, G. Cohen, and D. R. Reichman, Absence of diffusion in an interacting system of spinless fermions on a one-dimensional disordered lattice, Phys. Rev. Lett. **114**, 100601 (2015).

[42] K. Agarwal, S. Gopalakrishnan, M. Knap, M. Müller, and E. Demler, Anomalous Diffusion and Griffiths Effects Near the Many-Body Localization Transition, Phys. Rev. Lett. **114**, 160401 (2015).

[43] D. J. Luitz, N. Laflorencie, and F. Alet, Extended slow dynamical regime close to the many-body localization transition, Phys. Rev. B **93**, 060201 (2016).

[44] I. Khait, S. Gazit, N. Y. Yao, and A. Auerbach, Spin transport of weakly disordered Heisenberg chain at infinite temperature, Phys. Rev. B **93**, 224205 (2016).

[45] M. Žnidarič, A. Scardicchio, and V. K. Varma, Diffusive and Subdiffusive Spin Transport in the Ergodic Phase of a Many-Body Localizable System, Phys. Rev. Lett. **117**, 040601 (2016).

[46] D. J. Luitz and Y. B. Lev, The ergodic side of the many-body localization transition, Annalen der Physik **529**, 1600350 (2017).

[47] S. Bera, G. De Tomasi, F. Weiner, and F. Evers, Density Propagator for Many-Body Localization: Finite-Size Effects, Transient Subdiffusion, and Exponential Decay, Phys. Rev. Lett. **118**, 196801 (2017).

[48] M. Mierzejewski, J. Herbrych, and P. Prelovšek, Universal dynamics of density correlations at the transition to the many-body localized state, Phys. Rev. B **94**, 224207 (2016).

[49] M. Serbyn, Z. Papić, and D. A. Abanin, Thouless energy and multifractality across the many-body localization transition, Phys. Rev. B **96**, 104201 (2017).

[50] P. W. Anderson, Absence of diffusion in certain random lattices, Phys. Rev. **109**, 1492 (1958).

[51] N. F. Mott and W. D. Twose, The theory of impurity conduction, Advances in Physics **10**, 107 (1961).

[52] M. Schreiber, S. S. Hodgman, P. Bordia, H. P. Lüschen, M. H. Fischer, R. Vosk, E. Altman, U. Schneider, and I. Bloch, Observation of many-body localization of interacting fermions in a quasi-random optical lattice, Science **349**, 842 (2015).

[53] H. P. Lüschen, P. Bordia, S. S. Hodgman, M. Schreiber, S. Sarkar, A. J. Daley, M. H. Fischer, E. Altman, I. Bloch, and U. Schneider, Signatures of many-body localization in a controlled open quantum system, Phys. Rev. X **7**, 011034 (2017).

[54] M. Pandey, P. W. Claeys, D. K. Campbell, A. Polkovnikov, and D. Sels, Adiabatic eigenstate deformations as a sensitive probe for quantum chaos, Phys. Rev. X **10**, 041017 (2020).

[55] See Supplemental Material for details about Fig. 1, the role of the Lorentzian broadening, details about the fitting procedure and the Anderson LIOMs. It includes Refs. [17, 29, 38, 61, 64, 73, 85].

[56] K. Agarwal, E. Altman, E. Demler, S. Gopalakrishnan, D. A. Huse, and M. Knap, Rareregion effects and dynamics near the manybody localization transition, Annalen der Physik **529**, 1600326 (2016).

[57] D. J. Luitz and Y. Bar Lev, Anomalous thermalization in ergodic systems, Phys. Rev. Lett. **117**, 170404 (2016).

[58] S. Gopalakrishnan, K. R. Islam, and M. Knap, Noise-induced subdiffusion in strongly localized quantum systems, Phys. Rev. Lett. **119**, 046601 (2017).

[59] P. Prelovšek and J. Herbrych, Self-consistent approach to many-body localization and subdiffusion, Phys. Rev. B **96**, 035130 (2017).

[60] T. Chanda, P. Sierant, and J. Zakrzewski, Time dynamics with matrix product states: Many-body localization transition of large systems revisited, Phys. Rev. B **101**, 035148 (2020).

[61] P. Prelovšek, M. Mierzejewski, J. Krsnik, and O. S. Barišić, Many-body localization as a percolation phenomenon, Phys. Rev. B **103**, 045139 (2021).

[62] M. Kiefer-Emmanouilidis, R. Unanyan, M. Fleischhauer, and J. Sirker, Evidence for unbounded growth of the number entropy in many-body localized phases, Phys. Rev. Lett. **124**, 243601 (2020).

[63] M. Kiefer-Emmanouilidis, R. Unanyan, M. Fleischhauer, and J. Sirker, Slow delocalization of particles in many-body localized phases, Phys. Rev. B **103**, 024203 (2021).

[64] T. LeBlond, D. Sels, A. Polkovnikov, and M. Rigol, Universality in the onset of quantum chaos in many-body systems, arXiv:2012.07849.

[65] D. A. Huse, R. Nandkishore, and V. Oganesyan, Phenomenology of fully many-body-localized systems, Phys. Rev. B **90**, 174202 (2014).

[66] M. Serbyn, Z. Papić, and D. A. Abanin, Local conservation laws and the structure of the many-body localized states, Phys. Rev. Lett. **111**, 127201 (2013).

[67] V. Ros, M. Müller, and A. Scardicchio, Integrals of motion in the many-body localized phase, Nucl. Phys. B **891**, 420 (2015).

[68] A. Chandran, I. H. Kim, G. Vidal, and D. A. Abanin, Constructing local integrals of motion in the many-body localized phase, Phys. Rev. B **91**, 085425 (2015).

[69] J. Z. Imbrie, On many-body localization for quantum spin chains, J. Stat. Phys. **163**, 998 (2016).

[70] S. J. Thomson and M. Schiró, Time evolution of many-body localized systems with the flow equation approach, Phys. Rev. B **97**, 060201 (2018).

[71] G. De Tomasi, F. Pollmann, and M. Heyl, Efficiently solving the dynamics of many-body localized systems at strong disorder, Phys. Rev. B **99**, 241114 (2019).

[72] S. P. Kelly, R. Nandkishore, and J. Marino, Exploring many-body localization in quantum systems coupled to an environment via Wegner-Wilson flows, Nuc. Phys. B **951**, 114886 (2020).

[73] M. Mierzejewski, T. Prosen, and P. Prelovšek, Approximate conservation laws in perturbed integrable lattice models, Phys. Rev. B **92**, 195121 (2015).

[74] P. Prelovšek, J. Bonča, and M. Mierzejewski, Transient and persistent particle subdiffusion in a disordered chain coupled to bosons, Phys. Rev. B **98**, 125119 (2018).

[75] M. Mierzejewski, P. Prelovšek, and J. Bonča, Einstein relation for a driven disordered quantum chain in the subdiffusive regime, Phys. Rev. Lett. **122**, 206601 (2019).

[76] A. Dymarsky, Bound on eigenstate thermalization from transport, arXiv:1804.08626.

[77] M. Brenes, J. Goold, and M. Rigol, Low-frequency behavior of off-diagonal matrix elements in the integrable XXZ chain and in a locally perturbed quantum-chaotic XXZ chain, Phys. Rev. B **102**, 075127 (2020).

[78] T. LeBlond and M. Rigol, Eigenstate thermalization for observables that break Hamiltonian symmetries and its counterpart in interacting integrable systems, Phys. Rev. E **102**, 062113 (2020).

[79] A. D. Luca and A. Scardicchio, Ergodicity breaking in a model showing many-body localization, EPL (Europhysics Letters) **101**, 37003 (2013).

[80] D. J. Luitz, N. Laflorencie, and F. Alet, Many-body localization edge in the random-field Heisenberg chain, Phys. Rev. B **91**, 081103 (2015).

[81] N. Macé, F. Alet, and N. Laflorencie, Multifractal scalings across the many-body localization transition, Phys. Rev. Lett. **123**, 180601 (2019).

[82] D. E. Logan and S. Welsh, Many-body localization in fock space: A local perspective, Phys. Rev. B **99**, 045131 (2019).

[83] S. Roy and D. E. Logan, Fock-space correlations and the origins of many-body localization, Phys. Rev. B **101**, 134202 (2020).

[84] G. D. Tomasi, I. M. Khaymovich, F. Pollmann, and S. Warzel, Rare thermal bubbles at the many-body localization transition from the Fock space point of view, arXiv:2011.03048.

[85] J. Šuntajs, T. Prosen, and L. Vidmar, Spectral properties of three-dimensional Anderson model, Annals of Physics 168469 (2021).